NJC

ROYAL SOCIETY OF CHEMISTRY

PAPER

View Article Online
View Journal | View Issue

Cite this: *New J. Chem.*, 2024, **48**, 12266

Catalytic hydrogenolysis of lignin-derived compounds using sub-nanometer cobalt catalysts†

Miguel Cruz-González,[a] Lázaro Huerta[b] and Carmen Ortiz-Cervantes *[a]

Received 6th May 2024,
Accepted 13th June 2024

DOI: 10.1039/d4nj02124j

rsc.li/njc

In the quest for sustainable lignin valorization, the development of efficient catalytic systems for hydrogenolysis of lignin-derived compounds remains a pivotal focus. Utilizing sub-nanometer cobalt catalysts, we achieved the successful hydrogenolysis of model lignin molecules, including 1-(3,4-dimethoxyphenyl)-2-(2-methoxyphenoxy)ethanone and 2-(2,6-dimethylphenoxy)-1-(3,4-dimethoxyphenyl), resulting in the formation of highly efficient catalytic species characterized by high-angle annular dark-field scanning transmission electron microscopy (HAADF-STEM). Our catalyst exhibited remarkable recyclability over five cycles. Additionally, we conducted hydrogenolysis tests on authentic lignin samples, shedding light on the promising potential of this approach for sustainable lignin valorization.

1. Introduction

Each year, the quantity of lignocellulosic waste continues to rise steadily, yet a substantial portion of this resource remains underutilized for energy production. Fossil fuels persist as a dominant component in global primary energy usage, contributing to over two-thirds of greenhouse gas emissions. In response, the urgent need for an alternative, dependable, and environmentally sustainable energy source has become increasingly apparent. Lignocellulosic waste emerges as a viable raw material, offering the potential to generate renewable bioenergy.[1] Consisting of cellulose, lignin, and hemicellulose, lignocellulosic biomass encompasses agricultural and forestry residues such as crop stalks, straw, wood, and branches derived from both agricultural and commercial wood production sectors.[2]

However, the utilization of lignocellulosic waste for bioenergy encounters a significant hurdle due to the non-biodegradable nature of lignin.[3] Although techniques are employed to separate lignin from hemicellulose and cellulose, the challenge persists, leaving lignin as residual material. Among various methods, lignin hydrogenolysis stands out for its ability to occur under milder conditions – lower temperatures, neutral solutions, and shorter durations – yielding higher bio-oil yields and aromatic products. These conditions prove more economically viable, facilitating potential industrial-scale utilization.[4] Catalytic solvolysis and hydrogenolysis of lignin[5] and model lignin molecules are undoubtedly promising methods within lignin valorization.[6] The hydrogenolysis of bonds present in lignin, such as C–C and C–O, has recently been described through the oxidative photocatalytic cleavage of C–C and C–O bonds in lignin model molecules, either without the use of a metal catalyst[7] or with Earth abundant and low-cost metals such as cobalt, nickel,[8] iron, and manganese,[9] showing good yields.

Regarding the hydrogenolysis of model lignin molecules, in Table S2 of the ESI,† there is a comparison of the use of various catalysts for the hydrogenolysis of model lignin molecules, where catalysts such as Co-phen/C,[10] Pd/CeO_2,[11] and NiMo sulfide[12] stand out under somewhat similar conditions, but with different selectivity and temperatures around 200 °C.

To address the complexities of lignin depolymerization, the use of heterogeneous catalysts, particularly single-atom catalysts (SACs), emerges as a promising solution. SACs demonstrate efficacy in lignin valorization,[13] specifically targeting the cleavage of the β-O-4 bond,[14] a crucial step in the process.[15] Recent studies have highlighted cobalt SACs of the M–N–C type as particularly effective in the oxidative cleavage of the β-O-4 bond in lignin compounds, especially when using MeOH and NaOH as the solvent and additive, respectively.[16] Additionally, our group has previously elucidated the efficacy of sub-nanometric cobalt(II) species as catalysts for the hydrogenolysis of guaiacylglycerol-β-guaiacyl derivatives, demonstrating good conversion rates.[17]

In this context, this work focuses on synthesizing and evaluating single-atom cobalt catalysts, named **Co-1**, derived from cobalt acetate and 5-amino-1,10-phenantroline. These

[a] *Instituto de Química, Universidad Nacional Autónoma de México, CU, Coyoacán, 04510, Ciudad de México, Mexico. E-mail: carmen.ortiz@iquimica.unam.mx*
[b] *Instituto de Investigaciones en Materiales, Universidad Nacional Autónoma de México, CU, Coyoacán, 04510, Ciudad de México, Mexico*

† Electronic supplementary information (ESI) available. See DOI: https://doi.org/10.1039/d4nj02124j

catalysts, featuring isolated and dispersed metallic atoms on supports, hold promise for enhanced activity and selectivity. This thesis aims to present the outcomes of catalytic hydrogenolysis reactions conducted on model lignin molecules, pine, and kraft lignin using cobalt catalysts. The reactions are conducted in conjunction with hydrogen-donating molecules such as formic acid and alcohol/water mixtures, under varying molecular hydrogen pressures, achieving excellent yields and recyclability of the catalyst. This study holds the potential to drive advancements in catalytic systems, paving the way for the synthesis of renewable biofuels and chemicals through the utilization of precious-metal-free metal as efficient catalysts.

2. Experimental

2.1. Catalyst synthesis and characterization

The synthesis of the **Co-1** catalytic material was conducted as previously described,[17,18] in this work we utilized the ligand 5-amino-1,10-phenanthroline, as illustrated in Fig. 1A. Thus, to synthesize **Co-1**, a solution of $Co(OAc)_2{\cdot}4H_2O$ (0.073 g, 0.29 mmol) and 5-amino-1,10-phenanthroline (0.146 g, 0.75 mmol) in 25 mL of anhydrous ethanol was prepared in a 100 mL Schlenk flask. The mixture was sonicated for 10 minutes, followed by the addition of 1.6 g of MgO (nanopowder, particle size <50 nm), SEM image illustrated in Fig. 1b, and the flask was purged with argon. It was sonicated again for 10 minutes. The reaction mixture was placed in an oil bath at 60 °C for 12 h. The ethanol was removed by vacuum evaporation and allowed to dry for several hours under reduced pressure. After the solid reached the maximum possible dryness, 80 mg of the solid was transferred into borosilicate ampoules with a capacity of 1 mL, as illustrated in Fig. 1c. These ampoules were then sealed under vacuum to facilitate the subsequent heat treatment. The ampoules were heated at 600 °C for 2 h; during this process, the excess 5-amino-1,10-phenanthroline was carbonized. Following the heat treatment, an acid treatment was carried out with 45 mL of deionized water and 0.5 mol L^{-1} H_2SO_4 (1.187 mL). The purpose of the acid treatment is to eliminate the MgO template as well as any magnesium hydroxide that may have formed. The reaction mixture was left stirring and heating at 80 °C for 12 h. Once the mixture cooled, the solid was washed with distilled water until a neutral pH was reached. Finally, the material is dried under reduced pressure. The preparation of **Co-1** is illustrated in the scheme of Fig. 1a, and final **Co-1** solid is Fig. 1d.

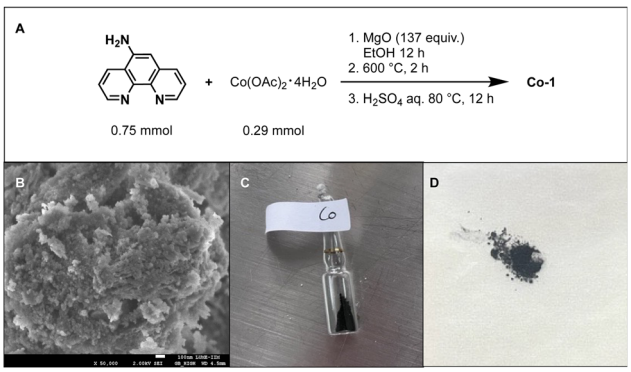

Fig. 1 (A) Synthetic procedure to obtain **Co-1** catalyst. (B) SEM image of magnesium oxide ($\leq$50 nm). (C) **Co-1** into borosilicate ampule after thermal treatment and (D) **Co-1** solid after acid treatment.

Then, diverse identification and characterization techniques were utilized for analyzing cobalt materials, alongside the organic compounds. Sample preparation adhered to detailed protocols outlined below for each set of materials.

For electron paramagnetic resonance spectra, solid samples were placed in quartz tubes of 1.34 cm diameter and 0.15 cm thickness. Loaded tubes were then introduced in a Jeol JES-TE300 spectrometer operating at X band frequency (9.4 GHz) at 100 kHz field modulation, with a cylindrical cavity (TE011 mode). Samples were run at 77 K. The ATR-IR spectra were determinate on a FTIR/FIR spectrum FT-IR NICOLET IS-50, Thermo Fisher Scientific, measuring 32 scans per sample, from 4000 to 400 cm^{-1} with a resolution of 2 cm^{-1}, the sample did not require previous preparation. Powder X-ray diffraction measurements were performed on a Rigaku Ultima IV diffractometer with Cu K_α radiation (l = 1.54056 Å) at 40 kV and 44 mA. The instrument was operating in a Bragg Brentano geometry with a step increment of 0.02° and an acquisition time of one second per step. Transmission electron microscopy studies were performed in a Jeol ARM-200F Cs-corrected microscope, operated at 200 keV using copper grids (mesh size of 300 covered with a lacey carbon film) equipped with a holey carbon. The samples were dispersed in anhydrous hexane. The SEM images were obtained in Jeol-SEM. XPS spectra were recorded at room temperature using a K-alpha + spectrometer Thermo Fisher Scientific Co. Equipped with an Al Ka (1486.6 eV) monochromatic X-ray source, a dual-beam flood gun for charge neutralization, and 180 double focusing hemispherical analyzer operating in a constant analyzer energy (CAE) mode. The measurement spot size was 400 μm and a base pressure of 1×10^{-9} mbar was held in the analytical chamber. Survey scans were recorded using 400 μm spot size and fixed pass energy of 200 eV, whereas high resolution spectra were recorded at 20 eV of pass energy with a step size of 0.1 eV. Charge corrections for all the spectra were referenced to the position of the C 1s adventitious peak at 284.8 eV. All spectra were processed with the Avantage software (v5.9925) provided by Thermo-Fisher Scientific Co. The curve fitting was performed with a Voight function and a Shirley-type background. Finally, elemental analysis of **Co-1** ware carried out in Thermo Scientific/Flash 2000. ICP-MS analysis for Co materials was measured using Thermo Scientific Element XR High-Resolution ICP-MS after digesting materials in aqua regia.

2.2. Catalytic performance

The conversion and selectivity of catalytic reactions were determined *via* GC-MS analysis performed on an Agilent 5975C system equipped with a 30 m DB-5MS capillary ((0.32 mm ID) column), He 99.999%.

2.2.1. Lignin model compounds hydrogenolysis with Et_3N/HCOOH. The hydrogenolysis reactions were carried out in

10 mL borosilicate tubes equipped with a stir bar and a Teflon cap, which were loaded with 1-(3,4-dimethoxyphenyl)-2-(2-methoxyphenoxy)ethanone, **S2** (40 mg, 0.13 mmol), 2 mL of EtOH, 2 mL of deionized water, and 15 mg of cobalt catalyst, triethylamine (92 μL, 0.66 mmol), and formic acid (14.99 μL, 0.39 mmol). The flask was purged with argon. Once the tube was sealed, it was placed in the Monowave at 180 °C for 2 h. After the reaction time, a thin-layer chromatography was performed for qualitative observation of the products. Solvents were evaporated, and the sample was dissolved in CH_2Cl_2 for GC-MS. Similarly, hydrogenolysis was performed for the **S2E** and **S3n**.

2.2.2. Catalyst recycling experiments. Catalyst recycling procedures involved the following steps: a prepared sample was subjected to hydrogenolysis reactions in 10 mL borosilicate tubes containing a stir bar and a Teflon cap. The tubes were loaded with **S2** (40 mg, 0.13 mmol), 2 mL of ethanol, 2 mL of deionized water, 15 mg of cobalt catalyst, triethylamine (92 μL, 0.66 mmol), and formic acid (14.99 μL, 0.39 mmol). The flask was purged with argon before sealing the tube, which was then placed in the Monowave at 180 °C for 2 hours. After the reaction, thin-layer chromatography was conducted to qualitatively observe the products. The solution was centrifuged for 20 minutes at 5000 rpm and washed three times with methanol.

2.2.3. Lignin model compounds hydrogenolysis with molecules hydrogen (H_2). Hydrogenolysis reactions were carried out in a 22 mL stainless steel Parr® reactor equipped with a magnetic stirrer. The reactor was loaded with **S2** (80 mg, 0.26 mmol), 20 mg of cobalt catalyst, 3 mL of EtOH, and 3 mL of deionized water. The reactor was sealed using its structure for purging with argon. Once the system was purged, a pressure gauge was installed to pressurize with H_2 gas to 10 bar. The reactor was placed at 180 °C for 24 h. After the designated reaction time, the products were qualitatively observed using a thin-layer chromatography plate. The reaction mixture was filtered to separate the catalyst from the product and remove the solvents. Finally, the dried sample was dissolved in CH_2Cl_2 for analysis by GC-MS. The same methodology was followed for the hydrogenolysis of **S2E** and **S3n**.

2.2.4. Lignin hydrogenolysis with Et_3N/HCOOH. Lignin depolymerization/hydrogenolysis reactions were carried out using the same methodology described previously. Initially, AF/Et_3N was used as a hydrogen source. This reaction was conducted in the Monowave, where a borosilicate tube was loaded with 50 mg of pine dioxasolv lignin or kraft lignin, 15 mg of **Co-1** catalyst, 2 mL of EtOH, 2 mL of deionized water, 14.99 μL of A.F, and 92 μL of Et_3N. The reaction mixture was placed in an argon atmosphere at 180 °C for 2 h. Once the reaction was complete, it was filtered to separate the catalyst from the reaction mixture. Solvents were evaporated, and the composition was analyzed using NMR and IR-ATR.

2.2.5. Lignin hydrogenolysis with hydrogen pressure. A Parr® reactor equipped with a magnetic stirrer was loaded with 50 mg of pine dioxasolv lignin or kraft lignin, 15 mg of **Co-1** catalyst, 3 mL of EtOH, and 3 mL of deionized water. The reactor was purged with argon, and a pressure gauge was used to pressurize it to 10 bar with H_2. The reaction was set at 180 °C for 24 h. After completion of the reaction, the mixture was filtered, and solvents were evaporated for subsequent composition analysis by NMR and FTIR-ATR

2.2.6. Lignin extraction. Lignin extraction was carried out according to a methodology reported previously,[19] briefly described below. In a solution of 30 g of softwood sawdust in a 1,4-dioxane/water mixture (9 : 1 vol./vol.) in the presence of 0.2 M hydrochloric acid, the mixture was refluxed at 90–95 °C under inert atmosphere for 4 h. The reaction mixture was allowed to cool, then filtered, and vacuum-concentrated using a rotary evaporator. Once concentrated, the dioxane-soluble lignin was isolated by precipitation in water, purified by precipitation in diethyl ether, and vacuum-dried to obtain dioxane-soluble lignin from softwood.

3. Results and discussion

3.1. Catalyst characterization

To gain valuable insights into the composition and morphology of the catalyst, we conducted a thorough structural analysis. The atomic composition of **Co-1**, determined through energy dispersive X-ray spectroscopy (EDS), revealed cobalt content of 0.3% atomic percent, while X-ray photoelectron spectroscopy (XPS) yielded a cobalt content of 1.3%. Elemental analysis further confirmed the presence of nitrogen (12.45%), carbon (60.43%), and hydrogen (3.14%). Additionally, inductively coupled plasma (ICP) analysis indicated a cobalt content of 0.54 wt%. The X-ray powder diffraction (XRD) analysis of the cobalt material revealed a broad diffraction peak at a 2θ value centered around 25°, as depicted in Fig. 2A. This peak is attributed to the carbon support resulting from the thermal treatment of the material; no peaks corresponding to magnesium oxide, or cobalt oxides are observed. According to Gul and colleagues,[20] similar peaks to those obtained when analyzing cobalt oxide are not present, and the absence of peaks is also attributed to the reduced metal loading. Additionally, the EPR spectrum only presents a signal with a *g*-value of 2.0023, attributed to carbon radicals originating from the support at 77 K, as illustrated in Fig. 2B. It is worth noting that signals for ferromagnetic cobalt species or for cobalt bound to cobalt nanoparticles, the presence of cobalt NPs can be ruled out, as according to the work described by the Beller group.[21]

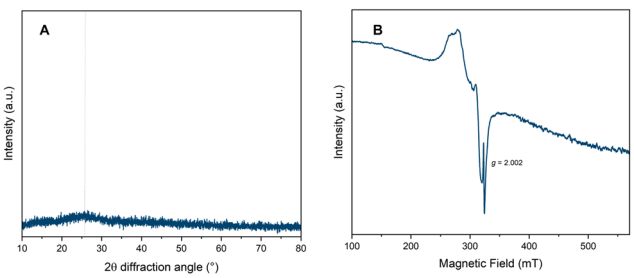

Fig. 2 (A) Powder X-ray diffraction (PDRX) patterns of **Co-1**, and (B) X-band electron paramagnetic resonance (EPR) spectra of **Co-1** solid.

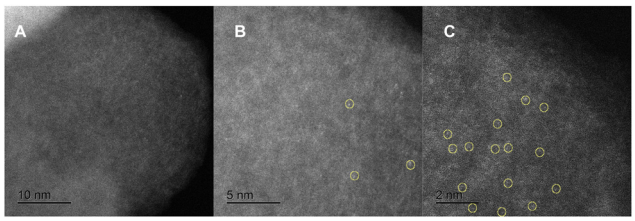

Fig. 3 HAADF-STEM images from freshly prepared **Co-1**, scale bars represent (A) 10 nm (B) 5 nm and (C) 2 nm. Yellow circles show brilliant points associate with cobalt atoms.

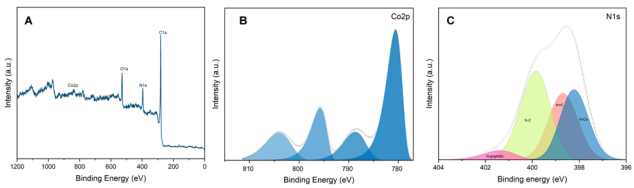

Fig. 4 (A) The survey XPS spectrum and high-resolution curve fitting for **Co-1** sample: (B) Co $2p_{3/2}$ and (C) N 1s XPS spectra.

To confirm that the **Co-1** catalyst corresponds to single-atom catalysts (SACs), STEM analysis was performed. Micrographs did not reveal the presence of nanoparticles, as shown in Fig. 3. These micrographs correspond to the **Co-1** material from the same batch, captured at varying magnifications, with dark-field imaging revealing small white dots representing cobalt atoms (enclosed in the circles). On the other hand, XPS spectra confirmed the cobalt oxidation state as 2^+, consistent with prior findings, and served as the foundation for spectrum fitting. Adjustments to the spectrum in Fig. 4B involved positioning the primary signal at 780.54 eV, alongside a satellite peak at 788.75 eV, confirming the presence of Co(II).[22,23] On the other hand, as depicted in Fig. 4C, the nitrogen atom exists in different chemical environments, with only a small fraction of the total nitrogen coordinated to cobalt at an energy of 398 eV.

3.2. Catalyst screening and optimization to S2 hydrogenolysis

To explore the efficacy of the **Co-1** catalyst in catalytic hydrogenolysis, we conducted a thorough screening and optimization process. The catalytic hydrogenolysis of **S2** was carried out using the **Co-1** catalyst, which proved effective for the C–O bond cleavage, yielding the products 1-(3,4-dimethoxyphenyl)ethan-1-one (A) and 2-methoxyphenol (B) with a conversion of 96% at 180 °C in 1 hour of reaction time (entry 1) and 99% in 2 hours. At 0.5 hours reaction time, a 16% conversion was obtained (entry 2), while at 1 hour, the conversion reached 96%. The reaction conditions at which maximum conversion was achieved were 2 hours with 2.8 mol% of cobalt (entry 4). Interestingly, as the temperature decreased, the conversion rate also decreased. For instance, at 170 °C, a conversion rate of 45% was observed, which was similar to that obtained at 150 °C. It's worth noting that hydrogen, necessary for the hydrogenolysis reaction, is obtained from the dehydrogenation of formic acid. Additionally, when triethylamine is not added to the reaction, the C–O bond cleavage in the **S2** molecule did not proceed, with the conversion being <1% (entry 10), as triethylamine plays a crucial role in deprotonating formic acid and leading to the formation of hydrogen. Studies conducted by the Beller group, utilizing highly dispersed cobalt catalysts (Co–N–C, Co(1)/phen(2)/C), concluded that such nanostructured cobalt catalysts exhibit good activity in formic acid dehydrogenation due to the formation of CoN_x species as active sites. However, the addition of an excess of phenanthroline (Co(1)/phen(7)/C) resulted in higher selectivity towards H_2 and CO_2, as well as the formation of individual cobalt atoms. Conversely, a lower loading of phenanthroline resulted in the formation of compact metallic Co particles.[24]

Triethylamine aids in the dehydrogenation of formic acid to act as a hydrogen donor molecule in the reaction, hence a significant decrease in conversion is observed in its absence. Additionally, with a homogeneous compound like $Co(PPh_3)_2Cl_2$, C–O bond cleavage was not achieved (entry 13), similarly in the absence of **Co-1** (entry 14).

Furthermore, poisoning experiments were conducted using thiocyanate ions (SCN^-) commonly employed as poisoning reagents to block the activity of metal-centered complexes under acidic conditions. When 5 mg of KSCN was used (entry 11), it was observed that the catalytic activity was not significantly affected, decreasing by only 4%, indicating that the **Co-1** catalyst may belong to the category of single-atom catalysts (SACs).

Additionally, poisoning tests were conducted with Hg. A study by the Ananikov group mentioned that the mercury test is one of the fastest methods to distinguish between truly homogeneous catalysts or metallic nanoparticles.[25] If the catalytic reaction is inhibited in the presence of Hg, it is considered evidence of nanoparticle formation; however, if there is no significant effect, it is considered a homogeneous catalyst, as metallic mercury will poison metal(0) nanoparticles acting as catalytically active centers while remaining inert to molecular metal complexes. As observed in entry 12 of Table 1, the addition of a drop of Hg (60.8 mg) did not result in a decrease in conversion, indicating that the **Co-1** catalyst may not consist of nanoparticles and is also categorized as a SAC, which aligns with microscopy findings.

Blank reactions were conducted in the absence of **Co-1**, and only nanostructured magnesium oxide was used, allowing for the observation of hydrogenolysis products in entries 14 and 15, respectively.

The optimal conditions for catalytic hydrogenolysis of **S2** were determined to be 180 °C for 2 hours, using 15 mg of catalyst. Subsequently, tests were conducted to evaluate the recyclability of the **Co-1** catalyst, which showed consistent good conversion and selectivity up to the fourth run but experienced a slight decrease in conversion during the fifth run, which is associated with the decrease in the amount of catalyst, as some gets stuck in the tube where the material is centrifuged. The results of the recycling runs are presented in Fig. 5A comparison with freshly prepared **Co-1** is shown in Fig. 6A, while the material observed after the fifth run is shown in Fig. 6B, where

Table 1 Catalytic hydrogenolysis of 1-(3,4-dimethoxyphenyl)-2-(2-methoxyphenoxy)ethanone (**S2**)

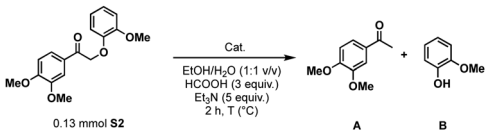

Entry	Conditions	Conv.[a] (%)	*A* (%)	*B* (%)
1	**Co-1** (3.7 mol%), 180 °C, **1 h**, HCOOH (3 equiv.), Et_3N (5 equiv.)	96	48	48
2	**Co-1** (3.7 mol%), 180 °C, **0.5 h**, HCOOH (3 equiv.), Et_3N (5 equiv.)	16	8	8
3	**Co-1** (**3.7 mol%**) 180 °C, 2 h, HCOOH (3 equiv.), Et_3N (5 equiv.)	99	50	49
4	**Co-1** (**2.8 mol%**), 180 °C, 2 h, HCOOH (3 equiv.), Et_3N (5 equiv.)	99	50	49
5	**Co-1** (**1.9 mol%**), 180 °C, 2 h, HCOOH (3 equiv.), Et_3N (5 equiv.)	96	48	48
6	**Co-1** (**0.9 mol%**) 180 °C, 2 h, HCOOH (3 equiv.), Et_3N (5 equiv.)	87	44	43
7	**Co-1** (2.8 mol%), **170 °C**, 2 h, HCOOH (3 equiv.), Et_3N (5 equiv.)	46	23	23
8	**Co-1** (2.8 mol%), **150 °C**, 2 h, HCOOH (3 equiv.), Et_3N (5 equiv.)	57	28	27
9	**Co-1** (3.7 mol%), **150 °C**, **3 h**, HCOOH (3 equiv.), Et_3N (5 equiv.)	40	20	20
10	**Co-1** (2.8 mol%), 180 °C, 2 h, HCOOH (3 equiv.)	<1	<1	<1
11	**Co-1** (2.8 mol%), 180 °C, 2 h, HCOOH (3 equiv.), Et_3N (5 equiv.) **KSCN (5 mg)**	95	48	47
12	**Co-1** (2.8 mol%), 180 °C, 2 h, HCOOH (3 equiv.), Et_3N (5 equiv.) **Hg (60.8 mg)**	99	50	49
13	**$Co(PPh_3)2Cl_2$** (4.1 mol%), 150 °C, 2 h, HCOOH (3 equiv.), Et_3N (5 equiv.)	0	0	0
14	180 °C, 2 h, HCOOH (3 equiv.), Et_3N (5 equiv.)	0	0	0
15	180 °C, 2 h, HCOOH (3 equiv.), Et_3N (5 equiv.), **MgO** (20 mg)	0	0	0
16	**Co-1** (2.8 mol%), 180 °C, 2 h, HCOOH (3 equiv.), Et_3N (5 equiv.) **TEMPO** (0.025 mmol, 20 mol%)	32	15	16

[a] All yields were determined by GC-MS with dibenzothiophene as standard.

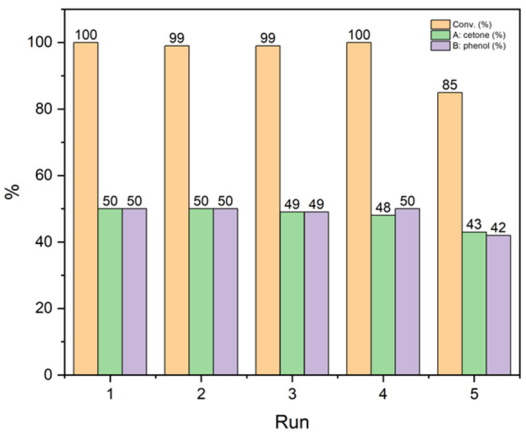

Fig. 5 **Co-1** catalyst recycling study in the hydrogenolysis of **S2**. Reaction condition: **Co-1**, EtOH : H_2O (2 mL : 2 mL), Et_3N (5 equiv.), HCOOH (3 equiv.) at 180 °C for 2 h of reaction.

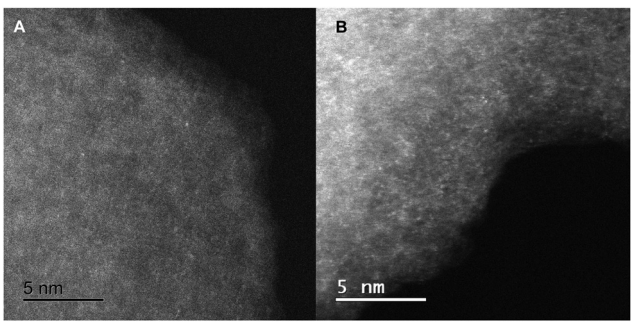

Fig. 6 HAADF-STEM images from (A) freshly **Co-1** and (B) **Co-1** after 5 runs, scale bars represent 5 nm.

no formation of nanoparticles is observed, but larger clusters are evident. The EDS of this material shows a lower cobalt content compared to the material initially used, Fig. S1B (ESI†).

Regarding the influence of solvents, as described in Table 2, it was observed that the mixtures H_2O/EtOH, H_2O/MeOH, and H_2O/^{i}PrOH proved to be the most effective in achieving good conversions. On the other hand, when using only isopropanol, a conversion of less than 50% was obtained, accompanied by the formation of dehydration products. When propylene carbonate was used as the reaction medium, the conversion was practically null. This suggests that H_2O/alcohol systems are more effective in the hydrogenolysis of **S2**, yielding good conversions, unlike when using only alcohol, such as isopropanol or propylene carbonate.

By analyzing the different hydrogen sources, good conversions were obtained when formic acid, isopropanol, and pressurized molecular hydrogen (10 bar, 24 h) were used. When employing 10 bar of pressurized H_2 at 150 °C with 0.26 mmol of **S2**, the amount of cobalt in entry 8 of Table 1 corresponds to 1.4 mol% of Co, obtaining a conversion similar to the AF/Et_3N system (entry 1).

It is worth noting that isopropanol showed an increase in conversion from 49% to 96% when KOH is added; however, the presence of products C and D remained. This means that adding a base promotes the C–O bond cleavage for **S2**. According to previous studies, adding NaOH also increases conversion and improves the cleavage of the β-O-4 bond.[16] This is due to transfer hydrogenation, in which the system consists of isopropanol acting as a hydrogen source and a base, in this case, potassium hydroxide, facilitating the C–O bond cleavage. However, the use of this system as a hydrogen source is not as efficient due to the formation of undesired products. This phenomenon arises from the transfer hydrogenation

Table 2 Catalytic hydrogenolysis of 1-(3,4-dimethoxyphenyl)-2-(2-methoxyphenoxy)ethanone (**S2**) with different hydrogen sources

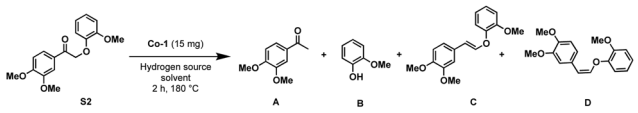

Entry	Hydrogen source	Conditions	Conv.[a] (%)	*A* (%)	*B* (%)	*C* : *D* (%)
1	HCOOH (3 equiv.)	2 h, Et_3N (5 equiv.) **S2** (0.13 mmol), EtOH : H_2O (1 : 1 v/v)	96	48	48	—
2	HCOOH (3 equiv.)	2 h, Et_3N (5 equiv.) **S2** (0.13 mmol), **^{i}PrOH : H_2O** (1 : 1 v/v)	99	50	49	—
3	HCOOH (3 equiv.)	2 h, Et_3N (5 equiv.) **S2** (0.13 mmol), **MeOH : H_2O** (1 : 1 v/v)	99	50	49	
4	HCOOH (3 equiv.)	2 h, Et_3N (5 equiv.) **S2** (0.13 mmol), **^{i}PrOH**	49	24	23	2 : 1
5	HCOOH (3 equiv.)	2 h, Et_3N (5 equiv.) **S2** (0.13 mmol)	0	0	0	—
6	^{i}PrOH (3 mL)	2 h, **KOH** (5 equiv.) **S2** (0.13 mmol)	96	41	41	11 : 3
7	Et_3SiH (3 equiv.)	24 h, MeCN, **S2** (0.13 mmol)	0	0	0	—
8	H_2 (10 bar)	**24 h**, EtOH : H_2O (3 mL : 3 mL) **S2** (0.26 mmol)	95	47	48	—
9	H_2 (10 bar)	**24 h**, 150 °C EtOH : H_2O (3 mL : 3 mL) **S2** (0.26 mmol)	94	47	47	—

[a] All yields were determined by GC-MS with dibenzothiophene as standard.

mechanism, wherein the system involves isopropanol serving as both a hydrogen source and a base, with potassium hydroxide facilitating the C–O bond cleavage. Nonetheless, the efficiency of this system as a hydrogen source is compromised by the formation of undesired products. Conversely, in the conditions outlined in entry 7, Et_3SiH did not demonstrate efficacy as a suitable hydrogen source.

3.3. Hydrogenolysis of lignin-related molecules

We next sought to determine the hydrogenolysis profile of lignin-derived species. The Table 3 shows the conversion of different model molecules previously synthesized, as well as the products obtained from catalytic hydrogenolysis under the established reaction conditions (180 °C, 2 hours, and 3 mol% cobalt). Entry 1 corresponds to the model molecule **S2**, showing good conversion, similar to entry 2, corresponding to the molecule **S2E**, which achieves 100% conversion.

Regarding entry 3, it pertains to the reaction with the molecule **S3n**, achieving a 5% conversion and failing to cleave the C–O bond. However, the reaction yields an etherification condensation product with ethanol.

Table 3 Catalytic hydrogenolysis lignin-related molecules

Entry	Substrate	Conv.[a] (%)	Products
1	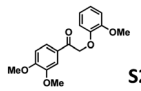 **S2**	99	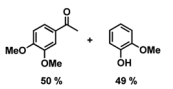 50 % 49 %
2	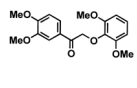 **S2E**	100	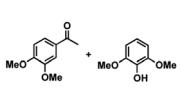 50 % 50 %
3	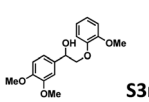 **S3n**	5	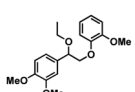 5 %

[a] All yields were determined by GC-MS with dibenzothiophene as standard. 3.0 mol% of **Co-1**. 2 h, HCOOH (3 equiv.), Et_3N (5 equiv.), substrate (0.13 mol), EtOH : H_2O (1 : 1 v/v), 180 °C, 2 h.

These outcomes are attributable to bond strength, as the presence of a carbonyl group, as in the molecules **S2** and **S2E**, necessitates less energy for breaking the C–O bond. Consequently, the molecule **S3n**, featuring a hydroxyl group, encounters greater difficulty in C–O bond cleavage due to its higher energy requirement. This aligns with the study described by the Beckham group,[26] which describes that bonds containing hydroxyl groups generally exhibit dissociation energies between 68.2 to 70.5 kcal mol^{-1}, whereas in the presence of carbonyl groups, the bond dissociation energy ranges from 50.7 to 60.6 kcal mol^{-1}.

Drawing upon these discoveries and preceding investigations,[27,28] we propose a reaction pathway for the breaking of C–O bonds in **S2**, outlined in Scheme 1. Initially, **S2** molecule coordinates with cobalt center through its oxygen atom (A) as recently described by Pratihar[29] according with *in situ* FT-IR spectra of carbonyl compounds.

Subsequently, as a product of the dehydrogenation of formic acid, hydrogen and carbon dioxide are generated. Previously, Beller's group[21] proposed the formation of cobalt hydride (B), a product of the homolytic cleavage of the dihydrogen molecule. For **Co-1** with formic acid, the formation of carbon dioxide, hydrogen, and carbon monoxide in very low concentration was detected, as observed in Fig. S36 (ESI†). Then, the C–O Sigma bond interacts with cobalt hydride (C), and the hydrogen atom is transferred to the C–O bond,[30] thus facilitating its cleavage leading to the formation of guaiacol and the

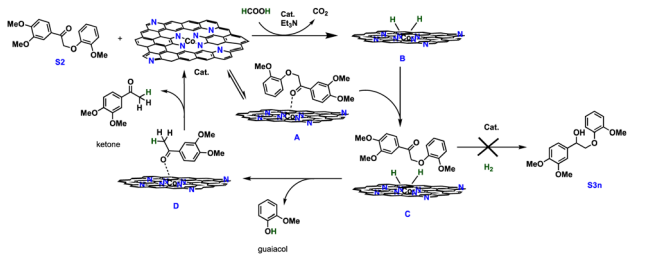

Scheme 1 Proposed reaction pathway to C–O bond cleavage catalyzed by **Co-1**.

corresponding ketone. The latter can coordinate to the metal center (D) and, once it dissociates, leads to the regeneration of the active catalytic cobalt species (Cat.) On the other hand, our experiments revealed that the hydrogenation of **S2** to form the **S3n** molecule does not occur in the presence of **Co-1** and hydrogen. Furthermore, under the same pressure and temperature conditions used for the hydrogenolysis of **S2**, the hydrogenolysis of **S3n** does not occur (entry 3, Table 3).

3.4. Hydrogenolysis of organosolv lignin and kraft lignin

We next studied the organosolv and kraft lignins. **Co-1** was employed to carry out the hydrogenolysis of lignin and to monitor its depolymerization using NMR and IR-ATR techniques. Fig. 7 shows the spectra generated by IR-ATR, comparing the dioxane-soluble lignin sample before hydrogenolysis. Upon analyzing the bands in detail, it corresponds to what has been described in publications by Liu and Zhang.[31,32] The presence of –OH groups are reported in the band around 3360 cm^{-1}, while carbon–hydrogen (CH_3 and CH_2) bonds are observed in the bands at 2929 and 2850 cm^{-1}. Around 1720 cm^{-1}, the band originates from the carbonyl group (C═O), including unconjugated ketone and carbonyl group stretching. The small band located at 1648 cm^{-1} is attributed to conjugated carbonyl stretching. In the region from 1560 to 1450 cm^{-1}, aromatic skeletal vibrations are attributed. The C–O bonds corresponding to the guaiacyl structure are located in the region from 1260 to 848 cm^{-1}, while bands corresponding to C–O bonds present in syringyl structures can also be found at 1316 and 1216 cm^{-1}, along with bands attributed to syringyl and guaiacyl structures in that region.

Additionally, the band at 1030 cm^{-1} corresponds to the deformation of C–O and primary alcohols or aliphatic ethers. The region from 900 to 500 cm^{-1} exhibits the coupling of signals that can be mono- to triply-substituted on the aromatic ring of lignin.

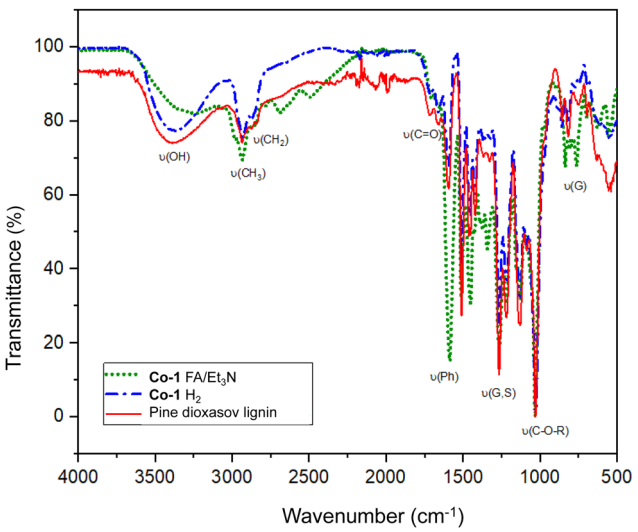

Fig. 7 ATR-FTIR spectra of the hydrogenolysis of pine dioxasolv lignin with 20 mg **Co-1**. 2 h, HCOOH (3 equiv.), Et_3N (5 equiv.), EtOH : H_2O (1 : 1 v/v), 180 °C, 2 h or under 10 bar of hydrogen pressure at 180 °C for 24 h.

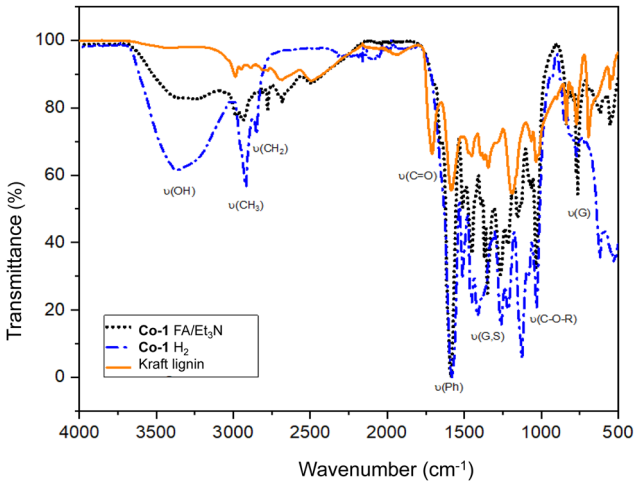

Fig. 8 ATR-FTIR spectra of the hydrogenolysis of kraft lignin with 20 mg **Co-1**. 2 h, HCOOH (3 equiv.), Et_3N (5 equiv.), EtOH : H_2O (1 : 1 v/v), 180 °C, 2 h or under 10 bar of molecular hydrogen (H_2) at 180 °C for 24 h.

The depolymerization and hydrogenolysis of kraft lignin were conducted utilizing the **Co-1** catalyst, Fig. 8. The FTIR-ATR spectra of kraft lignin before and after the reaction are presented. Given the established regions of the bands, the spectra can be elucidated by overlapping them, whether with the AF/Et_3N system or under hydrogen pressure (10 bar). In both scenarios, a change in –OH signals, as well as in methoxy groups, are discernible. For the reaction with hydrogen pressure, clearer signals of –CH_2 bonds are observed, as well as a greater quantity of signals associated with monolignols such as 2-methoxyphenol (guaiacol) and 2,6-dimethoxyfenol (syringol), as well as aromatic compounds.

The single-atom catalyst, notably the structured **Co-1** catalyst, has exhibited remarkable effectiveness in transforming model lignin molecules like 1-(3,4-dimethoxyphenyl)-2-(2-methoxyphenoxy)ethanone and 2-(2,6-dimethylphenoxy)-1-(3,4-dimethoxyphenyl) into their respective phenol and ketone counterparts. Furthermore, it shows promising potential as a catalyst for the hydrogenolysis of real lignin. Coordinated at nitrogen atoms, **Co-1** achieves C–O bond cleavage at 180 °C for a duration of 2 hours, concurrently catalyzing formic acid dehydrogenation and surpassing the productivity of all previously documented cobalt catalysts. Significantly, **Co-1** demonstrates outstanding catalytic durability, retaining its activity for over four cycles without notable deactivation. This exceptional performance of the cobalt catalyst is attributable to its distinctive Co–N_x species which stabilize its size at the single-atom level.

4. Conclusions

In summary, this study has focused on the synthesis of single-atom cobalt catalysts derived from cobalt acetate and 5-amino, 1,10-phenantroline. These catalysts, featuring isolated and

dispersed metallic atoms, hold promise for enhanced activity and selectivity in catalytic processes. Through extensive experimentation, this thesis has demonstrated the effectiveness of these cobalt catalysts in catalyzing hydrogenolysis reactions on model lignin molecules, as well as authentic pine and kraft lignin samples. By utilizing hydrogen-donating molecules like formic acid and alcohol/water mixtures, alongside varying molecular hydrogen (H_2), we have achieved outstanding yields of the desired products. Additionally, we propose a reaction pathway based on the findings and previously described reports. In our laboratory, further studies are being conducted to understand and provide evidence for the proposed mechanistic pathways of lignin hydrogenolysis and to comprehend the effect of the **Co-1** material structure. Furthermore, the successful recycling of the catalysts over multiple cycles underscores their potential for sustainable and efficient lignin valorization processes. In summary, this study has underscored the potential of single-atom cobalt catalysts in the hydrogenolysis of lignin-derived compounds. The successful recycling of the catalysts over multiple cycles further highlights their promise for sustainable and efficient lignin valorization processes, thus paving the way for broader applications in renewable resource utilization.

Author contributions

Carmen Ortiz-Cervantes: conceptualization, supervision and manuscript writing. Miguel Cruz-González: synthesis and catalysis and manuscript review. Lázaro Huerta: data analysis and manuscript review.

Data availability

The data, software, and code supporting the results presented in this manuscript are available upon request. All experimental data, including spectroscopic data and images from STEM are stored securely and can be provided upon request to the corresponding author. Software packages such as OriginPro, MestReNova and ChemDraw were utilized for data analysis and chemical structure depiction, respectively. Any necessary scripts or algorithms employed in data processing and analysis are available upon request. For inquiries regarding access to the data, software, or code supporting this work, please contact the corresponding author at carmen.ortiz@iquimica.unam.mx.

Conflicts of interest

There are no conflicts to declare.

Acknowledgements

We acknowledge the financial support from PAPIIT IA202023. We are also grateful to Virginia Gómez-Vidales (EPR), M. León and E. Tapia from Laboratorio Nacional de Ciencias Patrimonio Cultural LANCIC-IQ-UNAM, CONACYT (LN 232619, LN 260779, LN 279740, LN 293904, LN 271614 y LN 293904), Josue Romero and Rubén Mendoza (LUME, IIM), Elizabeth Huerta Salazar and Rubén Gaviño (NMR, IQ), María de la Paz Orta (EA, IQ), Adriana Romo (ATR, IQ), and Elizabeth Hernández Álvarez (ICP, IGEF) for technical assistance. We are grateful with Prof. Diego Solis-Ibarra, Prof. Juventino García for granting us access to several instruments.

References

1 R. Bellabarba, P. Johnston, S. Moss, C. Sievers, B. Subramaniam, C. Tway, Z. Wang and H. Zhu, *ACS Catal.*, 2023, **13**, 7917–7928.
2 P. Li, J. Ren, Z. Jiang, L. Huang, C. Wu and W. Wu, *RSC Adv.*, 2022, **12**, 10289–10305.
3 E. Subbotina and J. S. M. Samec, *Nat. Chem. Eng.*, 2024, **1**, 28–30.
4 X. Liu, F. P. Bouxin, J. Fan, V. L. Budarin, C. Hu and J. H. Clark, *ChemSusChem*, 2020, **13**, 4296–4317.
5 M. V. Galkin and J. S. M. Samec, *ChemSusChem*, 2014, **7**, 2154–2158.
6 C. Cheng, D. Shen, S. Gu and K. H. Luo, *Catal. Sci. Technol.*, 2018, **8**, 6275–6296.
7 Y. Meng, J. Li, H. Liu, H. Wu and H. Li, *Chem. Commun.*, 2024, **60**, 1642–1645.
8 P. Wu, L. Li, H. Li and Z. Fang, *Chem. Eng. J.*, 2024, **490**, 151722.
9 L. Li, P.-d Wu, W. Li, J. Huang, H. Li and S. Yang, *Small Struct.*, 2024, **5**, 2300531.
10 S. Rautiainen, D. Di Francesco, S. N. Katea, G. Westin, D. N. Tungasmita and J. S. M. Samec, *ChemSusChem*, 2019, **12**, 404–408.
11 Y. Hu, Y. Cui, S. Zhao, X. Zhao, X. Hu, Z. Song, W. Fan and Q. Zhang, *Green Chem.*, 2023, **25**, 5150–5159.
12 C. Zhang, H. Li, J. Lu, X. Zhang, K. E. Macarthur, M. Heggen and F. Wang, *ACS Catal.*, 2017, **7**, 3419–3429.
13 L. Chen, L. Pan, A. P. van Muyden, L. Bai, J. Li, Y. Tong, Z. Fei, A. Hagfeldt, G. Laurenczy and P. J. Dyson, *Cell Reports Phys. Sci.*, 2021, **2**, 100567.
14 T. Li, B. Chen, M. Cao, X. Ouyang, X. Qiu and C. Li, *AIChE J.*, 2023, **69**, 1–12.
15 S. De, A. S. Burange and R. Luque, *Green Chem.*, 2022, **24**, 2267–2286.
16 S. Liu, L. Bai, A. P. van Muyden, Z. Huang, X. Cui, Z. Fei, X. Li, X. Hu and P. J. Dyson, *Green Chem.*, 2019, **21**, 1974–1981.
17 D. Bautista-García, D. Macias-José, P. Aguillón-Rodríguez, O. Pérez-Reyes and C. Ortiz-Cervantes, *New J. Chem.*, 2023, **47**, 6164–6170.
18 W. Liu, Y. Chen, H. Qi, L. Zhang, W. Yan, X. Liu, X. Yang, S. Miao, W. Wang, C. Liu, A. Wang, J. Li and T. Zhang, *Angew. Chem., Int. Ed.*, 2018, **57**, 7071–7075.
19 S. Khviyuzov, M. Gusakova, K. Bogolitsyn and A. Volkov, *J. Wood Chem. Technol.*, 2021, **41**, 177–184.

20 I. Gul, S. M. Khan, T. Mehmood, Z. Ahmad, H. Badshah and H. Shah, *Microsc. Res. Tech.*, 2020, **83**, 1124–1131.
21 K. Stańczyk, R. Dziembaj, Z. Piwowarska and S. Witkowski, *Carbon N. Y.*, 1995, **33**, 1383–1392.
22 J. Yang, H. Liu, W. N. Martens and R. L. Frost, *J. Phys. Chem. C*, 2010, **114**, 111–119.
23 C. Tang, A.-E. Surkus, F. Chen, M.-M. Pohl, G. Agostini, M. Schneider, H. Junge and M. Beller, *Angew. Chem., Int. Ed.*, 2017, **56**, 16616–16620.
24 V. M. Chernyshev, A. V. Astakhov, I. E. Chikunov, R. V. Tyurin, D. B. Eremin, G. S. Ranny, V. N. Khrustalev and V. P. Ananikov, *ACS Catal.*, 2019, **9**, 2984–2995.
25 X. Li, A.-E. Surkus, J. Rabeah, M. Anwar, S. Dastigir, H. Junge, A. Brückner and M. Beller, *Angew. Chem., Int. Ed.*, 2020, **59**, 15849–15854.
26 S. Kim, S. C. Chmely, M. R. Nimlos, Y. J. Bomble, T. D. Foust, R. S. Paton and G. T. Beckham, *J. Phys. Chem. Lett.*, 2011, **2**, 2846–2852.
27 M. Nichols, L. M. Bishop, R. G. Bergman and J. A. Ellman, *J. Am. Chem. Soc.*, 2010, **132**, 16725.
28 J. Luo, X. Zhang, J. Lu and J. Zhang, *ACS Catal.*, 2017, **7**, 5062–5070.
29 J. Mishra, P. Mrugesh, P. S. Subramanian and S. Pratihar, *Inorg. Chem.*, 2024, **63**, 10423–10433.
30 M. Mensah, R. Tia, E. Adei and N. H. de Leeuw, *Catalysts*, 2023, **13**, 757.
31 J. Zhang, H. Deng, L. Lin, Y. Sun, C. Pan and S. Liu, *Bioresour. Technol.*, 2010, **101**, 2311–2316.
32 J. Hu, R. Xiao, D. Shen and H. Zhang, *Bioresour. Technol.*, 2013, **128**, 633–639.

